ISSN 0024-4902, Lithology and Mineral Resources, 2019, Vol. 54, No. 5, pp. 374–389. © Pleiades Publishing, Inc., 2019.
Russian Text © The Author(s), 2019, published in Litologiya i Poleznye Iskopaemye, 2019, No. 5.

Tectonic-Sedimentary System of the Atlantis–Meteor Seamounts (North Atlantic): Volcanism and Sedimentation in the Late Miocene–Pliocene and Position in the Atlantic–Arctic Rift System

N. P. Chamov[a], *, I. E. Stukalova[a], S. Yu. Sokolov[a], A. A. Peive[a], N. V. Gor'kova[a], A. A. Razumovskii[a], M. E. Bylinskaya[a], and L. A. Golovina[a]

[a] *Geological Institute, Russian Academy of Sciences, Pyzhevskii per., 7, Moscow, 119017 Russia*

**e-mail: nchamov@yandex.ru*

Received February 19, 2019; revised February 19, 2019; accepted March 13, 2019

Abstract—The paper analyzes original data obtained on the Atlantis–Meteor seamount system during Cruise 33 of the R/V *Akademik Nikolai Strakhov* in the eastern North Atlantic. This system is a volcanic rise formed on the Canary abyssal plate and represents one of the key objects for understanding the geological history of opening of the central segment of the Atlantic Ocean. Basalts, tephrites, and organogenic terrigenous lagoonal marine sediments dredged from the Atlantis, Plato, and Cruiser seamounts are considered. Petrography and compositions of the Atlantis and Cruiser basalts reflect significant differences in settings of their eruptions. Well-crystallized vesicle-free olivine basalts from the Atlantis Seamount were ejected under deep-water conditions. Glassy vesicular basalts of the Cruiser Seamount are typical of shallow subaerial eruptions. Evidence for the accumulation of tuff breccias and tuff gravelstones of the Plato Seamount in subaerial settings are obtained. Tendencies were revealed in the lithogenetic transformations of organogenic–terrigenous sediments of the Cruiser Seamount, which were subjected to the high-temperature impact of subaerial lava flows. During the volcanosedimentary lithogenesis, the plant lignite-like matter lost its primary structure and was transformed into anisotropic coke with the wide development of fusinite and pyrofusinite. The studied volcanic occurrences are thought to be related to the final (Late Miocene–Pliocene) volcanic stage in the seamount system, which predated the destruction of the system, its prograde subsidence, and transformation of islands into guyots.

Keywords: North Atlantic, seamount, tectonics, sedimentation

DOI: 10.1134/S0024490219050043

INTRODUCTION

Geological Position and Characteristics of the Seamount System

The tectonic-sedimentary system of the Atlantis–Meteor seamounts is a regional crustal element, which represents a single volcanic rise formed on the Canary abyssal plate and is one of the key objects for understanding the geological history of the North Atlantic opening (Fig. 1).

The volcanic rise is situated about 1500 km to the northwest of Africa, marked by 3750-m isobath, has a length no less than 1000 km, and area over 350000 km^2. It comprises seven large flat-topped seamounts presently located at depths from 240 to 800 m. The sublatitudinal Oceanographer, Hayes, and Atlantis fracture zones intersecting the Mid-Atlantic Ridge are terminated in the area of the Atlantis, Cruiser, and Great Meteor seamounts, respectively.

In spite of the comprehensive investigations since 1970s, views on the evolution of the Atlantis–Meteor seamounts are contradictory. The existing models can be divided into two principle groups: hot spots and structural control.

According to the first concept, the systems of the Corner and Atlantis–Meteor seamounts in the west and east of the North Atlantic, respectively, mark the subsequent passage of the North American plate, Mid-Atlantic Ridge, and African plate over the New England hotspot in the Late Cretaceous (Tucholke and Smoot, 1990). However, this concept cannot offer a satisfactory explanation of the resumption of volcanism on some seamounts 20–30 Ma after their initial passage over the hotspot. Inferred plate rollback or possible relation of the hot spot with the previously formed volcanic edifices through some intralithospheric channels a few kilometers thick is not geologically substantiated.

Models of this group also ignore the fact that the Atlantis–Meteor seamount system has a complex morphology, which cannot be explained in the framework of a single system of geodynamic strains. The

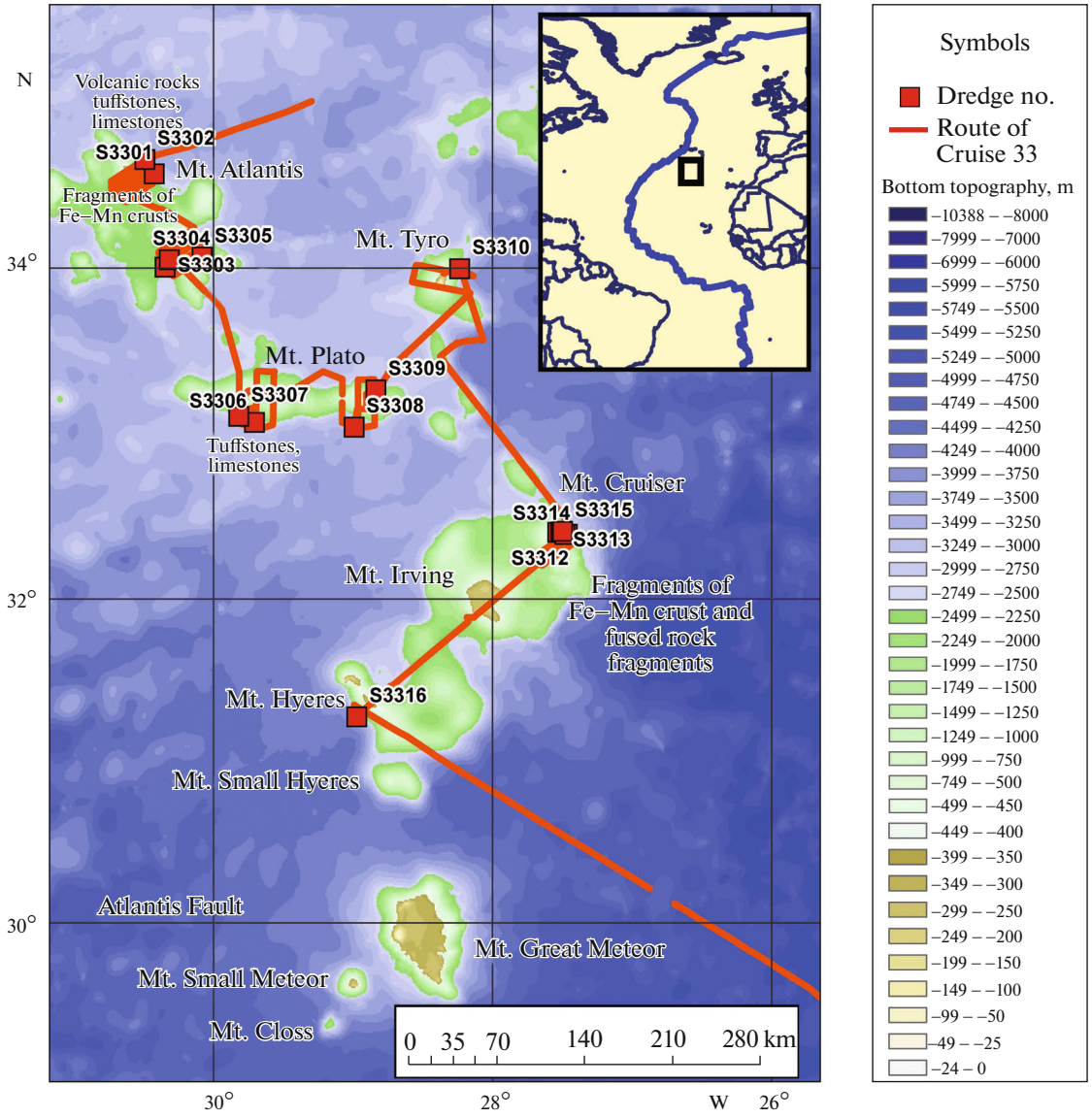

Fig. 1. Scheme of the performance of geological–geophysical works during Cruise 33 of the R/V *Akademik Nikolai Strakhov* in the Atlantis–Great Meteor area. Compiled using GEBCO data of 30″ Bathymetry Grid. Version 2014-11-03. 2014 (http://www.gebco.net). Red line is the cruise track. Rectangles are the position of dredging stations. Inset shows the position of the studied area in the Atlantic.

position of seamounts (Fig. 1) indicates the existence of at least four structural axes: northwestern (Atlantis Plateau, Cruiser–Tyro, Great Meteor–Hyeres); northeastern (Plato–Tyro–Unnamed, Hyeres–Irving–Cruiser); latitudinal (Plato); and the least pronounced sublongitudinal (Great Meteor–Hyeres).

Models of the second group are based on the kinematic mechanism of the formation of the seamount system and on the structural control of "hot" anomalies detected by seismic tomography data (Bebeshev et al., 1989; Georgen, 2011). Similar models relate the evolution of the region with large-scale interaction between the spreading ridge and the Azores plume (Gente et al., 2003; Ribeiro, 2017).

Geologists from the Geological Institute of the Russian Academy of Sciences studied the Atlantis–Great Meteor seamount system during Cruises 1 (1985) (Bebeshev et al., 1984) and 33 (2016) of the R/V *Akademik Nikolai Strakhov*. This paper reports the results of the macro- and microscopic study of the volcanic and terrigenous–humic rocks dredged from seamount slopes during 2016 expedition (Fig. 1). New materials supplement data on the nature of volcanic rocks obtained during Cruise 1 and highlight previously unknown features of the volcanosedimentary

Table 1. Station, coordinates, and depths of the beginning and end of dredging

Station no.	Initial latitude	Initial longitude	Final latitude	Final longitude	Initial depth, m	Final depth, m
S3302	34°36.4′	−30°33.7′	34°36.0′	−30°34.0′	840	800
S3307	33°11.5′	−29°49.0′	33°12.4′	−29°42.2′	1500	1260
S3312	32°23.0′	−27°30.0′	32°23.5′	−27°30.6′	1800	1670

lithogenesis of terrigenous–humic sediments under the impact of high-temperature subaerial lava flows.

Timing of the Seamount Formation

Based on the interpretation of magnetic anomalies (Verhoef, 1984), ocean floor beneath the seamounts are dated at 82–86 Ma for the Great Meteor, 75–83 Ma for Hyeres, 69–78 Ma for Irving, 68–77 Ma for Cruiser, 49–60 Ma for Plateau, 50–56 Ma for Tyro, and 37–48 Ma for Atlantis.

The formation of volcanic buildups began no earlier than Oligocene or early Miocene (Willians et al., 1983). Based on the K-Ar dating, the age of dredged basalts is 33.4 ± 0.5 Ma for Plato and 31.6 ± 0.4 Ma for Small Hyeres (Ribeiro et al., 2017). The age of the Cruiser seamounts calculated using empirical curves of the subsidence of the Atlantic Ocean crust is about 16 Ma (Tucholke and Smoot, 1990). The minimum age for the Cruiser–Hyeres seamount complex is estimated to be 13.3 Ma (Duin, 1984). Based on the K-Ar dating of basalts from depths of 600 and 1000 m, the minimum age of the Great Meteor seamount is 16.3 ± 0.4 and 10.7 ± 0.5 Ma, respectively (Wendt et al., 1976).

Their Miocene age also follows from the microfaunal analysis of samples dredged from seamount slopes during Cruise 1 of the R/V *Akademik Nikolai Strakhov.* All sedimentary rocks dredged from the slopes of the volcanic rises are enriched in the organogenic carbonate. Most of the rocks are organogenic limestones consisting of remains of foraminiferal shells, organogenic carbonate detritus, and nannoplankton (Golovina et al., 1984).

The **Atlantis seamount** was dredged at different slopes and depths. The lower part of its slope (depth up to 2340 m) yielded detrital limestones consisting of foraminiferal shells and nannoplankton embedded in the fine-clastic calcite cement. Nannoplankton is represented by the following species: *Coccolithus pelagicus* (large miocenica forms), *C. aff. macintyrei*, and *Discoaster deflandrei* (extreme overgrowing by secondary $CaCO_3$). Based on these forms, the age of the limestones was determined approximately as Miocene (23–5 Ma). Among the dredged samples are also foraminiferal–detrital limestones with nannoplankton of Quaternary age (*Calcidiscus macintyrei* and finest *Gephyrocapsa* sp.).

Samples collected from the middle part of the Atlantis slope (depth about 2000 m) contain diverse warm-water relatively shallow assemblage: *Reticulofenestera pseudoumbilicus*, *Sphenolithus* sp., *Scyphosphaera* sp.sp. (3 or 4 species), *Discoaster surculus*, *D. brouweri*, *D. aff. berggrenii*, *D. prepentaradiatus*, *Amaurolithus* aff. *primus* (1 specimen.), *Ceratolithus rugosus* (1 specimen), and others. All discoasteraceae excessively overgrown by calcite are poorly identified; given this fact, host rocks could be dated by the second half of the Late Miocene (Golovina et al., 1984).

Thus, the age of the organogenic rocks from the Atlantis slopes spans a stratigraphic interval from Oligocene to Quarter. Sedimentation occurred in a warm relatively shallow setting and was accompanied by the redeposition of products of the simultaneous volcanic activity (Bebeshev et al., 1989).

The **Cruiser Seamount** is characterized by the wide development of diverse organogenic limestones. The limestones from the western slope at a depth of 1800–1300 m yielded nannoplakton assemblage with *Coccolithus pelagicus*, *Discoaster deflandrei*, *D. exilis*, *Calcidiscus macintyrei*, *D.* aff. *kugleri*, *D.* aff. *bellus,* and other forms of the lower Middle Miocene (15–11 Ma)—*Discoaster exilis* zone (Golovina et al., 1984).

The **Great Meteor seamount** is overlain by the cover (150–600 m) of post-Middle Miocene (<11 Ma) carbonate and pyroclastic rocks and sands (Bebeshev et al., 1989). According to studies (Mironov and Krylova, 2006), the summit surface during the Late Miocene–Pliocene (11–2 Ma) was subjected to marine abrasion and then subsided to a depth about 300 m, which terminated the reef formation.

RESULTS

General Characteristics of Dredged Rocks

During 2016 expedition, the stony material was dredged from the slopes of the Atlantis, Plato, and Cruiser seamounts. Dredging parameters are given in Table 1.

Station S3302 on the northeastern slope of Atlantis yielded volcanic rocks, tuffstones, and limestones (Fig. 2a).

The basalts are greenish gray and dense. On the saw-cut section, separate crystals of olivine or iddingsite pseudomorphs after olivine are observed in a homogenous groundmass. It is noteworthy that practically unaltered and completely replaced crystals occur in a close vicinity to each other in a dense homogenous matrix. The crystals have both equant

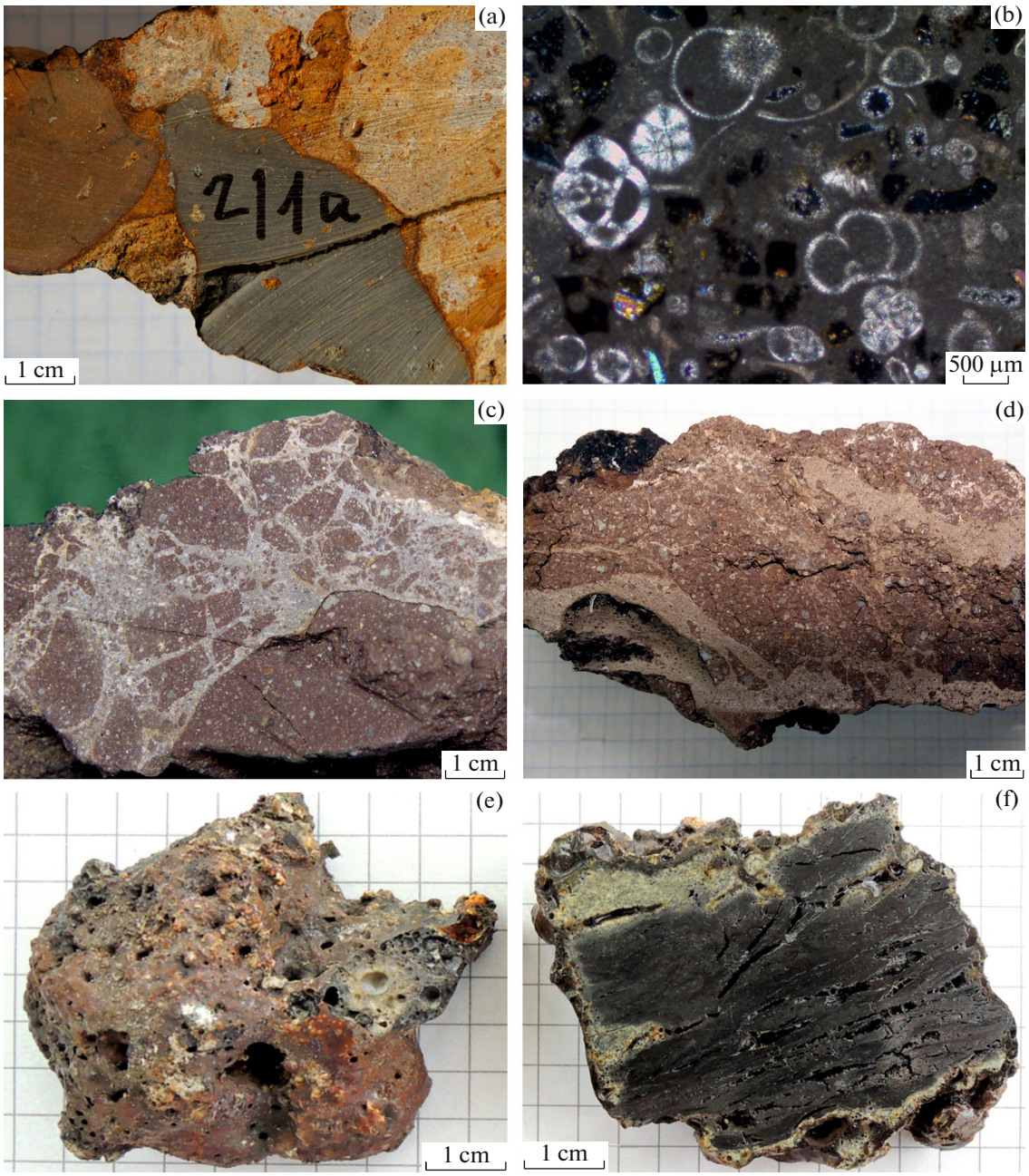

Fig. 2. Dredged rocks. (a, b) Atlantis seamount, station S3302: (a) contact between basalt and carbonate rocks, (b) mixture of volcaniclastics and bottom sediments, polished thin section, crossed nicols; (c, d) Plato seamount, station 3307: (c) tuff breccia, (d) tuff gravelstone; (e, f) Cruiser seamount, station S3312: (e) outer side of sample S3312-3 (variegated glassy rock with porous structure), (f) polished section of sample S3312-3 (greenish gray glassy fringe with embayments around dark lignite-like material).

and elongated shape. Equant olivines reach 0.5–0.7 cm in size.

Chill margins and intense ferrugination as tongues penetrating in a carbonate mass at the contact between basalts and limestones indicate the hot contact between lava and sediment in the past (Fig. 2a). Carbonate sediments at the contact with basalts are saturated in microfaunal remains of a wide taxonomic diversity (Fig. 2b). Planktonic foraminifers are represented by *Orbulina universa*, *Globorotalia menardii*, *G. crassaformis*, *G. tumida*, *G. scitula*, *G. puncticulata*, and *Globigerina bulloides*, which are typical of the Miocene–Pliocene.

Station S3307 from the southern slope of Plato seamount yielded volcanomictic, locally brecciated reddish brown rocks of variable density (Fig. 2c). The

main part of the rocks is made up of irregularly shaped randomly oriented fragments varying in size from 1 to 5 cm. The fragments have massive structure and fine gravelly texture. The grains are volcanomictic and weakly rounded, while the cement is tuffogenic and basal. Within brecciation zones, the fragments acquire angular shape, while their size varies from 1 cm to a few millimeters. The light cement has a calcareous composition and intensely liberates CO_2 when treated with HCl. The absence of microfaunal remains in the cement suggests a chemogenic nature of the carbonate.

Rocks of similar composition but different facies are represented by the weakly cemented fine pebbly gravelstones, which breakdown manually and bear signs of viscous rock flow (Fig. 2d). Mixing of incoherent mass in the past is emphasized by irregularly shaped sandy–carbonate interbeds up to 1 cm thick. The fragments show a good gradational sorting (0.2–0.4 cm) and are poorly rounded. The cement is volcanogenic–sandy fine-grained, and equigranular.

Station S3312 on the eastern slope of the Cruiser seamount yielded ferromanganese crusts and irregularly shaped nodules of fused porous rocks (Fig. 2e). It is seen in the saw-cut polished sections that they are mainly made up of the dark rock resembling wood coal, which is enveloped in a greenish gray glassy coat (Fig. 2f). The glassy coat strongly varies in thickness from a few millimeters to 1 cm and penetrates into the predominant rock along interlayers and "embayments." It is clearly seen that the glassy fringe is also developed on the internal surface of elongated cavities in the coalified material. Physical properties of the observed varieties are sharply different: the glassy rock is hard and leaves no mark, whereas the dark rock is easily crabbed by nail or knife and leaves a black mark on a streak plate.

Below we present the results of microscopic study of the dredged rocks.

Basalts

Basalts of the Atlantis seamount (station S3302) have a well-crystallized microlitic texture and are practically devoid of vesicles, indicating that the melt crystallized at relatively high pressures (Fig. 3a). Phenocrysts account for about 10–15%. They are mainly represented by large (usually 0.5–3 mm, up to 5 mm) olivine crystals of both octahedral and elongated prismatic or elongated drop-shaped (quench crystals) shape. Olivine is locally replaced by iddingsite, which sometimes forms complete pseudomorphs. Single clinopyroxene phenocrysts reach 5 mm. The groundmass is weakly crystallized. It is made up of small (about 0.1 mm) plagioclase laths, olivine microlites (0.25 mm), and vitrified glass. Small rounded ore minerals (0.05–0.1 mm) compose up to 30% matrix.

The presence of sharply elongated olivine (quench crystals) indicates its rapid crystallization during magma eruption. Traces of magmatic flow are expressed by the deflection of microlites around phenocrysts. In addition, basaltic eruption on seafloor is confirmed by the entrapment of mud material saturated in microfaunal remains in a lava flow (Figs. 3a, 3b). Significant temperature difference at the lava–sediment contact follows from the clear chill margins around the entrapped material. Basaltic eruptions at great depth of Mt. Atlantis are determined from much wider diversity of the entrapped microfaunal assemblage as compared to the reduced subaerial assemblage of Cruiser.

In **Cruiser samples** (station S3312), glassy rocks under microscope reveal the characteristic features of lava flows. The groundmass has a typical hyalopilitic (felty) texture with plagioclase microlites embedded in a glassy matrix. The rock has an amygdaloidal structure typical of shallow subaerial eruptions, which produce relatively thin clearly vesicular hyalobasaltic flows. Numerous amygdules are filled with thin plagioclase microlites, more rarely, with ferruginous aggregate containing pyroxene microcrystals (Fig. 3c). Abundant ore minerals are frequently developed along amygdule periphery (Figs. 3c, 3f). The amygdules vary from rounded to droplike and completely shapeless. The droplike amygdule filled with palagonitized glass (Fig. 3d) contains clear traces of viscous–ductile flow with tension cracks typical of pahoehoe lavas. Macroscopically observed penetration of glassy lava in the lignitic mass and flow structures are also observed under microscope (Fig. 3e). Chill margins are weakly developed, although they are observed on separate contact areas and around some detrital grains. Lava mobility is also supported by the inclusions of host rocks. A relatively large foraminiferal shell seen in the polished thin section (Fig. 3f), judging from the absence of pores and arrangement of chambers, can be approximately determined as the representative of Miliolida. This is benthic group inhabiting relatively shallow depths. The finest calcareous interbed in sample S3312-3 contains single coccolithic species *Calcidiscus leptoporus* (Murray and Blackman 1898; Loeblich and Tappan, 1978), the stratigraphic range of which is determined from the base of the Acvitanian (19.00–22.82 Ma) to the present time.

Tuff Breccia

In **samples from Mt. Plato (station S3307)**, we studied polished thin sections of massive rock varieties that compose tuff breccia (Fig. 4).

The fragments are represented by the angular fine to medium-grained basalts with diverse texture, or, more rarely, by altered minerals. Brown tuffaceous–clay matrix is strongly ferruginated. Ore minerals are widespread both in the matrix and in basaltic fragments. Sometimes, segregations of ore minerals are confined to lithophysis–cavities formed by air bubbles (Fig. 4d).

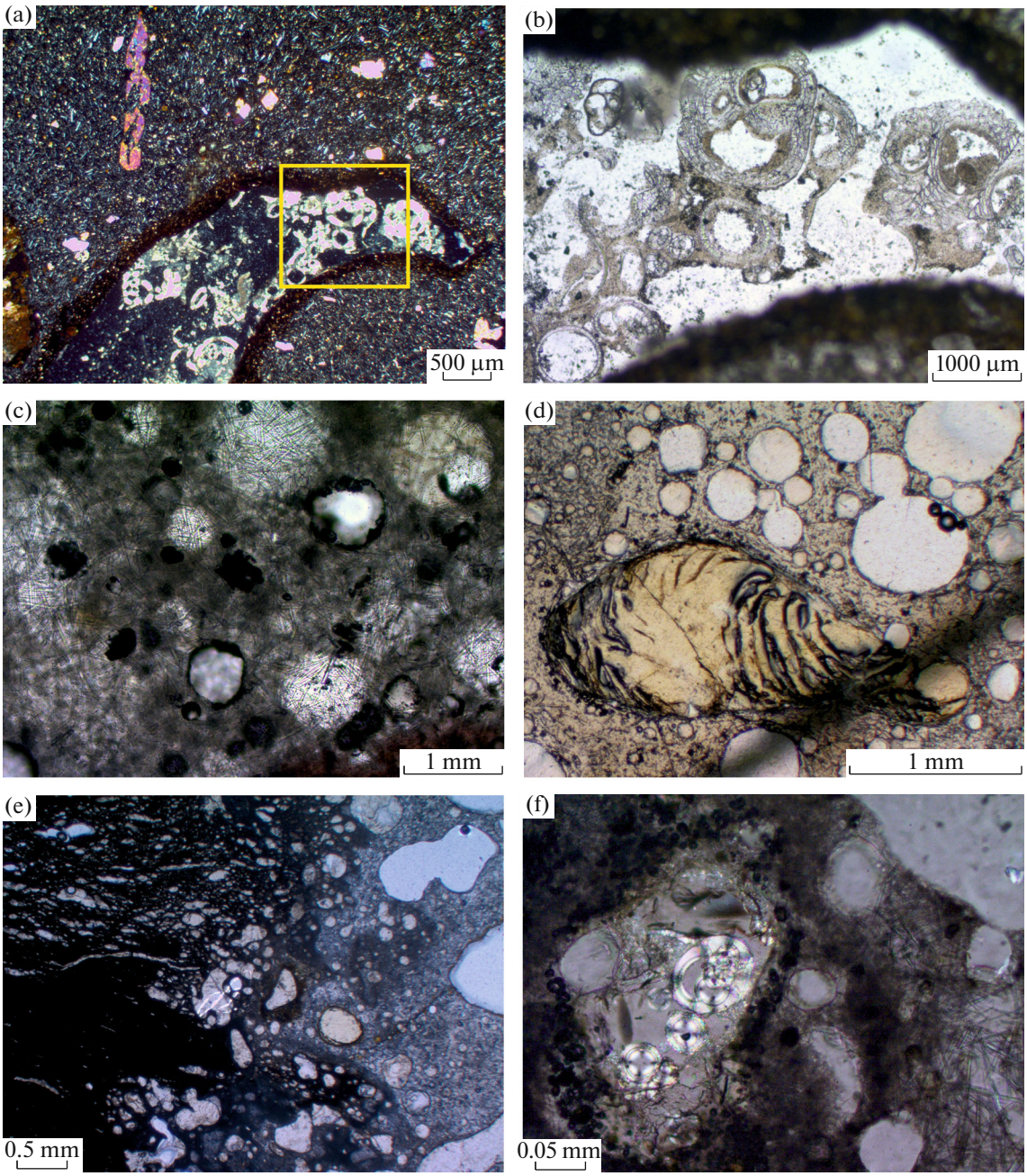

Fig. 3. Lava flows of the Cruiser and Atlantis seamounts. (a, b) Atlantis, station S3302: (a) microlitic olivine basalt, crossed nicols, (b) microfauna-bearing bottom sediments entrapped by lava flow (fragment of polished thin section outlined by yellow frame in Fig. 3a, parallel nicols); (c–f) Cruiser seamount, station S3312: (c) glassy amygdaloidal basalt, crossed nicols, (d) flow textures in a deformed vesicle, parallel nicols, (e) contact of lava flow with organogenic–sedimentary rocks, crossed nicols, (f) microfaunal remains in the irregularly shaped amygdule, crossed nicols.

Directive textures, flow traces, sorting, as well as microfauna inclusions are absent. Based on the observations, the tuffaceous material was formed from a pyroclastic flow erupted in subaerial conditions.

According to (Ribeiro et al., 2017), tephrites were also dredged from the northern slope of Mt. Cruiser.

Terrigenous–Humic Sediments

Station S3312, Mt. Cruiser. Under optical microscope, the groundmass composing the central parts of the considered nodules has a clearly stratified texture formed by the alternation of plant humic and pelitic terrigenous materials (Fig. 5a).

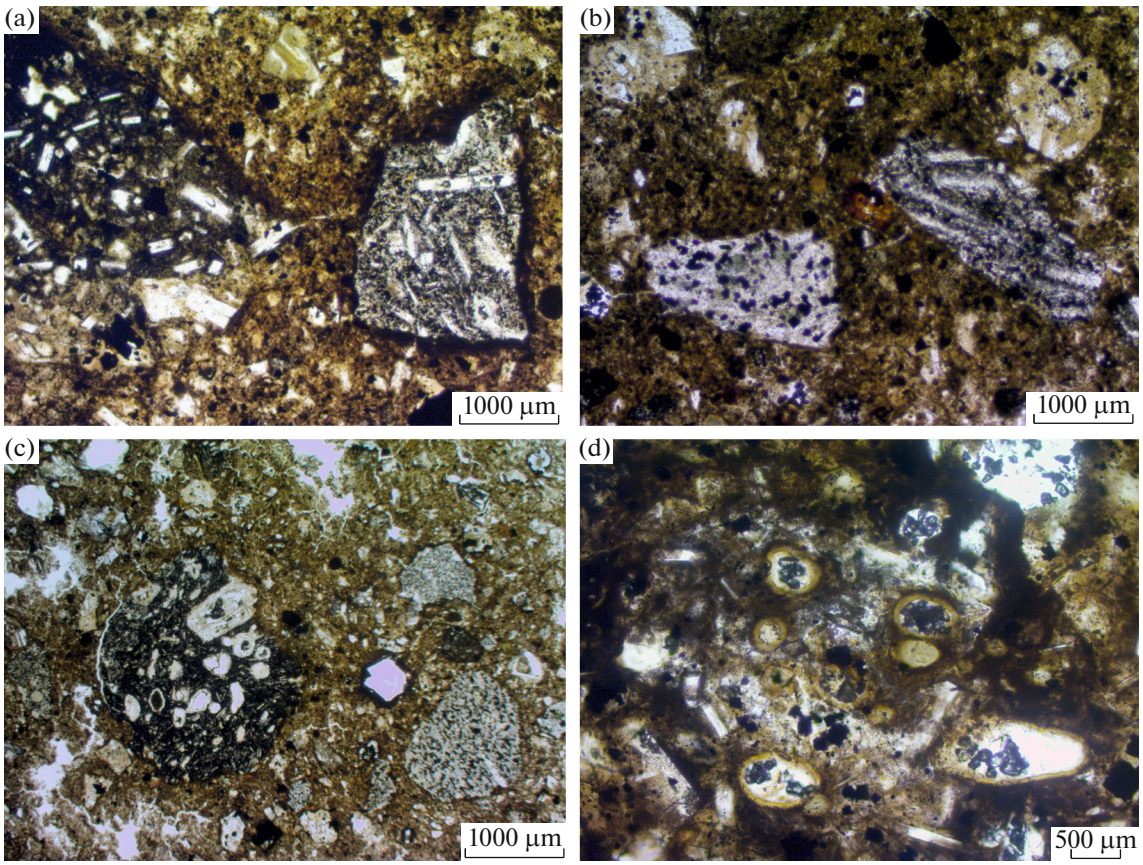

Fig. 4. Tuffogenic sediments of the Plato seamount, station S3307.

The terrigenous grains are poorly and mildly rounded, and the largest grains reach 0.5 mm across. The thickness of terrigenous interbeds varies from 0.01 to 1.0 mm.

Both terrigenous and humic interbeds usually have a lenticular shape. They are frequently disrupted by strike with shear displacement of fragments. The disruption of stratification is also expressed in the formation of pinch zones, where interlayers are deformed and transformed into melange (Fig. 5b). The terrigenous interlayers contain microfaunal remains: cysts of calcic dinoplagellates, benthic foraminifers, and calcic algae (Figs. 5c, 5d).

In spite of the general structural similarity with lignites, the plant humus in the transmitted light has a black color, which is not typical of lignites. Lignites usually have brown or light brown color. Obvious humification of humic organic matter indicates its high-temperature transformation. Early studies showed that even short-term thermal impact of erupted volcanic material on the organic matter of terrestrial vegetation leads to the sharp and uneven changes of its composition and properties (Petrova et al., 1998; Stukalova et al., 2004). An increase of temperature stimulates the condensation and ordering of carbonaceous structure, which is accompanied by a change of mass, compaction, and reduction of volume (shrinkage).

The influence of high-temperature lavas and solutions on the transformation (lithogenesis) of humic matter from station S3312 of Mt. Cruiser was studied under high magnification with optical and scanning microscopes. It is seen in Fig. 6a that volcanogenic–hydrothermal rock saturates the laminated humic matter. Interlayers are split by the intruding material. Organogenic matter acquires porous texture, transforming into a natural coke. A change of primary structure of vitrinite microcomponents facilitates the formation of pores and cavities, which imparts the pumice-type appearance (Fig. 6b). The groundmass retains the relicts of plant matter.

Bands of structural vitrinite with clear cellular structure split by vertical cracks are seen under small magnifications (about 100 times) (Fig. 6c). Thermal impact caused the transformation of vitrinite microcomponent into another microcomponent, micrinite (agglomerate of organic and mineral matter). The organic matter contains large and small fragments of fusinite. Under large magnifications (200–500 times) and, especially, in oil immersion, micrinite bands are converted into a mineral mass saturated with the fine and finest particles of gray vitrinite and fusinite, which

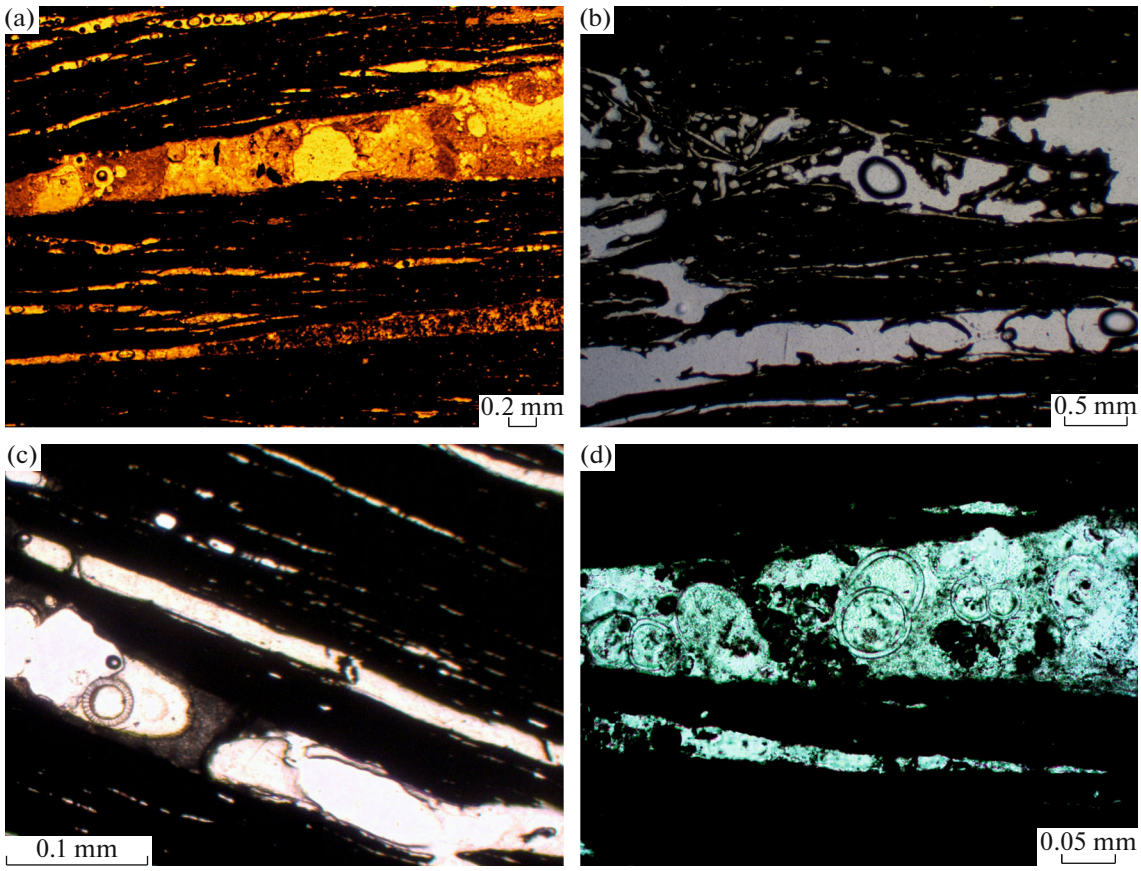

Fig. 5. Terrigenous–humic sediments of the Cruiser seamount, station S3312. (a) Humic material opaque in the transmitted light with terrigenous interbeds; (b) disruption of stratification in the laminae pinch zone; (c) single calcium cyst of Dinoflagellata in a terrigenous interbed; (d) calcite algae in terrigenous interbed.

is distinguished by angular shape and bright white color. Fusinite is transformed into pyrofusinite, which shows clear strong mosaic anisotropy (Stach et al., 1978). Vitrinite is destroyed into small fragments and is replaced by the pyroclastic material. The value of refraction index Ro in the separate microcomponents of vitrinite group increases significantly and becomes more than 3%. It is practically impossible to measure the value of refraction of micrinite microcomponent owing to the presence of the finest organic particles, which look like spanglets in the volcanic material.

Figure 6d shows a clear cellular structure of plant tissues: dark fields in the images are the mineral volcanogenic hydrothermal matter, which saturated the plant remains; gray fields are the micrinite microcomponent; and bright white fields are stellate segregations of fusinite and pyrofusinite. The typically lignite structure of the plant tissues indicates a terrestrial origin of the fragments of humic material and makes it possible to relate it with the higher plants (trees and shrubs).

Electron microscopic study revealed numerous deformation structures in the organogenic–terrigenous thin-laminated sediments (Fig. 7). They are expressed in the bed disruptions (Figs. 7a, 7c), boudinage, and brecciation on a different scale (Figs. 7b, 7d), formation of convolute structures (Fig. 7b), and appearance of sandy dikes (Fig. 7a).

Chemical Composition of Terrigenous–Humic Rocks

The contents and spectra of elements in the terrigenous–humic sediments were determined on a CamScan MV2300 scanning electron microscope coupled with INCA200 for the energy-dispersive X-ray microanalysis.

A significant increase of carbon content was established in terrigenous varieties. In recalculation for oxides, the CO_2 content in the externally terrigenous varieties ("light") is strongly overestimated, exceeding in some cases 50% (Table 2).

In the dark (humic) varieties, the carbon content reaches 95–100%, with sharply subordinate amounts of N, Al, Si, and O (Table 3). the obtained values confirm the concept (based on microstructural study) that the rock is natural coke.

Following assumptions can be made from the X-ray microanalysis with allowance for the laminated tex-

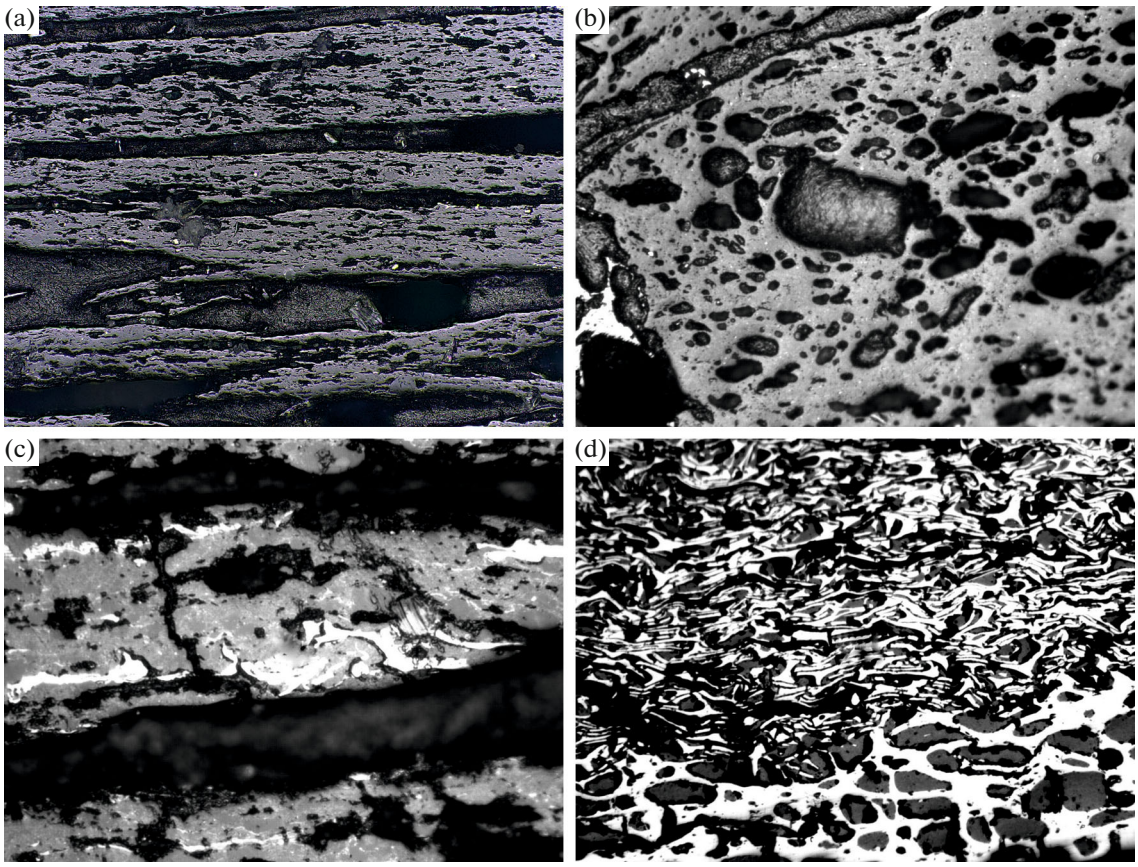

Fig. 6. Types of the transformation of humic material from the Cruise Seamount, station S3312. (a) Welding and shrinkage of the humic matter during injection of the volcanogenic material; polished section, reflected light, magn. 100; (b) porous texture of micrinite, reflected light, immersion, magn. 100; (c) vitrinite bands, micrinite, fragments of fusinite, reflected light, immersion, magn. 100; (d) clear cellular texture of plant tissues: dark fields show the saturation of plant remains in the mineral volcanogenic–hydrothermal material; gray fields are microcomponent micrinite; bright white fields are stellate segregations of fusinite and pyrofusinite, polished section, reflected light, oil immersion, magn. 200.

ture of the rocks. The thermal impact on lignite matter made up mainly of the higher plant fragments leads to the redistribution of components. Thermal reworking caused a removal of volatiles and mobile components from the lignite organogenic material and its transformation into the highly carbonaceous coke. Mobile CO_2-saturated fluids saturated the laminas with the terrigenous and likely sapropel material, thus facilitating the leaching and redeposition of some components. The removal of Fe, Ca, Na, Si and, to lesser extent, K was accompanied by the enrichment in CO_2 (Table 2).

Table 2. Chemical composition of light interbeds in the terrigenous–humic sediments, wt %

Sample	SiO_2	Al_2O_3	FeO^t	MgO	CaO	Na_2O	K_2O	CO_2	Total
S3312/t14	46.67	10.17	0	1.06	0	3.84	3.17	35.09	100.00
S3312/t17	63.84	0.73	0	0	0	0	0	35.43	100.00
S3312/t21	35.52	8.76	0	0.74	0	1.19	2.14	51.56	99.91
S3312/t22	30.78	12.24	1.08	0.5	0	0.15	1.95	53.3	100.00
S3312/t25	47.95	10.33	0	0.95	0	0	3.28	37.5	100.01
S3312/t26	32.53	14.73	0	0.53	0	0	1.89	50.34	100.02
S3312/t46c	55.78	1.19	0	2.05	4.64	9.04	0.65	26.65	100.00

Analyses were carried out on a SEM CamScan MV2300, gold sputtering. Position of measurement points is shown in Figs. 7a–7c.
FeO^t as total iron.

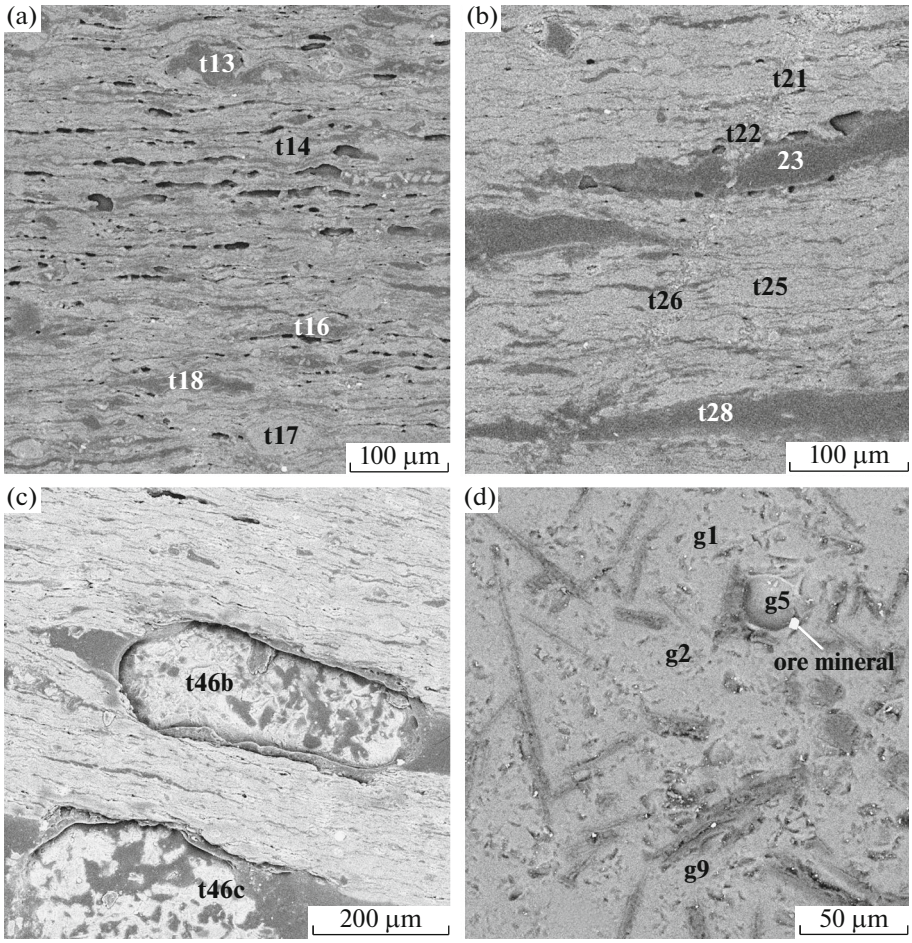

Fig. 7. Results of the electron microscopic study of terrigenous–humic and volcanic rocks of the Cruiser Seamount, station S3312. (a–c) Deformation structures in the terrigenous–humic rock; (d) hyalopilitic structure of basalt. Indices show the measurement points of rock composition on a CamScan MV 2300 scanning microscope coupled with INCA 200 for the EDS X-ray microanalysis. Chemical composition in the measurement points is shown in Tables 2–4.

This tendency is best expressed in measurements t21, t22, and t26 along the sandy dike that obliquely crosscuts the subhorizontal stratified terrigenous–humic sediments (Fig. 7b). They demonstrate a sharp (18–30%) decrease of SiO_2 at proportional growth of CO_2 (Table 2). This observation reflects the mobility of highly reactive fluids and their selective confinement to the weakened zones of the rock.

Although the presence of glassy coat around the terrigenous–humic rocks seems to be the ground for the isochemical conditions of volcanosedimentary lithogenesis, the existing data are insufficient to substantiate the geochemical closure of the system. At the same time, significant part of the redistributed mineral material has remained within the system. In particular, among newly formed minerals are abundant high-Fe ore minerals, which are identified under electron microscope as small bright white grains dispersed in a stratified mass (Figs. 7a, 7b, 7d).

Chemical Composition of Basalts

Basalts of the Atlantis and Cruiser seamounts significantly differ from each other in the degree of alteration, which affected the chemical compositions and choice of the study method.

Basalts of the Atlantis seamount have a fresh appearance and can be analyzed by the XRF method (Table 4). The obtained compositions in general are typical of within-plate alkali volcanic rocks. In the $Na_2O + K_2O$ vs. SiO_2 discriminant diagram (LeBas et al., 1986), data points of volcanic rocks are restricted to the boundary between basanites and picrite basalts. In the $Na_2O + K_2O$–MgO–FeO_{total} diagram (AFM) (Irvine and Baragar, 1971), they are grouped in the field of calc-alkaline rocks. The Fe mole fraction (f' = $FeO + Fe_2O_3 + MgO + TiO_2$) in lava flows varies within 22–25.

Basalts of the Cruiser Seamount were previously studied during Cruise 1 of the R/V *Akademik Nikolai Strakhov*. Analysis of the chemical composition

showed that all studied volcanic rocks were subjected to significant postmagmatic alterations, which were accompanied by intense transformation of their primary chemical composition (Zolotarev et al., 1984). The main chemical transformations in the rocks are related to the significant Si removal, insignificant Mg loss, and significant increase of the Fe content. In addition, the rocks have high P_2O_5 contents (up to 10 wt %), which is not typical of unaltered magmatic rocks. Zolotarev et al. attempted to reconstruct the chemical composition of volcanic rocks by recalculating the compositions of altered rocks with subtracting the formula amounts of apatite and calcite. However, the comparison of calculated compositions of strongly altered rocks with the bulk composition of basalts of the Atlantis seamounts does not seem correct.

Contents and spectra of elements in the basalts from station S3312 were determined using CamScan MV2300. The hyalopilitic texture of rocks is best expressed under electron microscope: plagioclase microlites are usually separated from each other by glass (Fig. 7d). The major element of the microlites is Al (80–100%), while Si, Fe, Mg, and Ca occur in subordinate amounts.

Ore minerals observed as bright white grains under electron microscope form numerous small and single porphyritic crystals in a glassy matrix. Large crystal has the following composition (Fig. 7d) (in wt %): FeO 71.4, SiO_2 5.27, Al_2O_3 3.1, and SO_3 0.23.

Representative measurements of the composition of glassy matrix of the basalts are shown in Table 4. In the $Na_2O + K_2O$ vs SiO_2 discriminant diagram (LeBas et al., 1986), data points of matrix of Mt. Cruiser volcanic rocks define a continuous basalt–basaltic andesite–andesite series. In the $Na_2O + K_2O$–MgO–FeO_{total} (AFM) diagram (Irvine and Baragar, 1971), their data are grouped in the field of calc-alkaline rocks. The Fe mole fraction (f' = FeO + Fe_2O_3 + MgO + TiO_2) in lava flows is no more than 16, which corresponds to their mesocratic appearance.

Obviously, direct comparison of the bulk compositions of the Atlantis basalts and the glassy matrix of the Cruiser basalts is incorrect. In addition, the low alkali content in the Cruiser basalts is likely related to secondary alterations. However, the complex of observations indicates that the calc-alkaline rocks of both volcanic buildups belong to the single trachybasalt–trachyandesite series.

DISCUSSION

Volcanic and Sedimentation Settings in the Miocene

The same bathymetric levels at different flanks of the seamount system point to a subsynchronous subsidence of all parts of the volcanic rise. Flat-topped peaks suggest the involvement of the volcanic buildups in a zone of high hydrodynamic activity.

Table 3. Element composition of dark interbeds in the terrigenous–humic sediments

Sample	Element	wt %	at %
S3312/t13	C	89.88	91.90
	O	7.04	5.40
	N	3.08	2.70
S3312/t16	C	92.94	94.69
	O	6.77	5.18
	Al	0.29	0.13
S3312/t16	C	77.88	83.71
	O	17.53	14.15
	Si	3.13	1.44
	Al	1.46	0.70
S3312/t23	C	83.40	86.29
	O	9.19	7.13
	N	7.42	6.58
S3312/t28	C	92.12	93.96
	O	7.88	6.04

Analyses were carried out on a SEM CamScan MV2300, with gold sputtering. Position of measurement points is shown in Figs. 7a, 7b.

Evidently, erosion accompanied the prograde subsidence of the volcanic rise. It is reasonable to suggest that before this stage, the peaks of volcanic buildups have emerged above sealevels. Analysis of the modern morphostructure and depth of the Cruiser seamount suggests that initially the seamount have raised 400–500 m above sea level (Bebeshev et al., 1984).

The study of terrigenous–humic sediments points to the subaerial sedimentation settings in the past. The laminated texture of the organogenic–terrigenous mass indicates its multiple accumulations in a semi-isolated shallow-water basin with periodical influx of the terrigenous material and plant fragments. The sediments are mainly made up of fragments of the terrestrial higher plants (remains of shrubs and tree branches), which follows from the clear cellular texture of plant tissue. The contribution of shallow–marine plant material (calcareous algae or algal mats) was insignificant.

Partial isolation of the basin from ocean follows from a poor taxonomic composition of microfauna. The absence of traces of active water dynamics and the pelite size of terrigenous material serve as evidence in favor of the quiescent sedimentation setting. Such conditions could exist in a shallow bay (lagoon), which served as a local depocenter for the adjacent volcanic buildups.

Tuffaceous sediments of the Plato Seamount do not contain fragments of marine microfauna in the cement and were likely formed under subaerial conditions. Tuff breccia was formed owing to the compac-

Table 4. Bulk chemical composition of Atlantis basalts and glassy matrix of Cruiser basalts, wt %

Sample	SiO_2	TiO_2	Al_2O_3	Fe_2O_3	FeO	MnO	MgO	CaO	Na_2O	K_2O	P_2O_5	L.O.I.	Total
Atlantis seamount													
3302/b1a	39.58	3.99	15.66	7.18	5.87	0.17	7.63	11.66	2.61	0.64	0.70	3.67	99.35
3302/b1b	39.49	4.07	17.47	6.74	5.83	0.18	6.22	11.54	2.85	0.55	0.92	3.50	99.36
3302/b1c	40.94	3.98	15.38	8.14	4.84	0.17	7.46	11.51	2.92	0.84	0.64	2.65	99.46
3302/b3	38.97	4.14	15.29	7.31	6.13	0.19	7.45	12.01	2.88	0.82	0.60	3.54	99.33
Cruiser seamount													
3312/g1	55.44	1.30	25.56	0.00	7.87	0.00	2.48	3.07	0.39	3.89	0.00	0.00	100.00
3312/g2	55.41	0.88	24.31	0.00	8.60	0.00	3.01	3.59	0.61	3.59	0.00	0.00	100.00
3312/g5	57.24	1.64	24.95	0.00	5.99	0.00	2.04	4.01	0.56	3.57	0.00	0.00	100.00
3312/g9	57.95	0.00	22.77	0.00	7.97	0.00	2.84	3.83	0.80	3.84	0.00	0.00	100.00
3312/g15	54.75	1.06	24.81	0.00	8.34	0.00	2.66	4.00	0.44	3.94	0.00	0.00	100.00
3312/g16	58.46	1.37	21.64	0.00	6.57	0.00	1.67	4.35	0.69	5.24	0.00	0.00	99.99
3312/g17	54.00	1.33	23.47	0.00	8.68	0.00	2.48	4.53	1.54	3.97	0.00	0.00	100.00
3312/g18	56.12	1.60	23.27	0.00	7.38	0.00	2.71	4.25	0.45	4.22	0.00	0.00	100.00
3312/g19	55.55	0.96	22,52	0.00	7.88	0.00	2.67	4.27	0.42	4.30	1.43	0.00	100.00
3312/g20	56.02	1.87	22.90	0.00	8.38	0.00	2.07	3.49	0.70	3.71	0.87	0.00	100.01
3312/g21	54.97	1.18	22.86	0.00	8.61	0.00	2.66	4.39	0.63	3.68	1.04	0.00	100.02
3312/g22	52.13	1.28	20.97	0.00	8.06	0.00	1.86	4.42	0.48	3.96	2.24	4.61	100.01
3312/g23	55.17	0.57	23.82	0.00	8.14	0.00	2.88	4.36	0.84	3.92	0.29	0.00	99.99
3312/g24	55.20	1.34	23.13	0.00	8.69	0.00	2.40	3.88	0.73	4.05	0.59	0.00	100.01
3312/g25	52.84	1.44	21.48	0.00	8.10	0.00	2.10	3.76	0.49	3.75	1.43	4.60	99.99
3312/g26	53.80	1.53	23.64	0.00	8.71	0.00	2.10	4.00	0.94	3.85	1.43	0.00	100.00
3312/g27	54.45	1.27	24.14	0.00	9.30	0.00	1.76	3.91	0.76	3.69	0.71	0.00	99.99
3312/g28	55.05	0.96	23.47	0.00	9.19	0.00	2.53	4.09	0.64	4.01	0.07	0.00	100.01
3312/g29	54.32	1.23	24.10	0.00	8.14	0.00	2.22	4.33	0.82	4.06	0.79	0.00	100.01
3312/g30	55.16	1.73	23.56	0.00	7.86	0.00	2.06	3.72	0.92	4.09	0.89	0.00	99.99

The chemical composition of basaltic samples S3302/b1a–S3302/b3 was analyzed by the XRF; the chemical composition of glassy matrix of basaltic samples 3312/g1–3312/g30 was determined on a SEM CamScan MV2300, coal sputtering. Position of measurement points 3312/g1–3312/g9 is shown in Fig. 7d.

tion and cementation of the nonsorted coarse-clastic loose volcaniclastic material in the sand-sized tuff cement. Facies similarity of tuff gravelstones with the alluvial–proluvial sediments of temporal water streams also serves in support of the subaerial sedimentation settings.

Previous study showed that the Cruiser Seamount was formed in two volcanic stages (Bebeshev et al., 1984). The first stage was marked by the submarine eruption of practically vesicle-free ankaramite–hawaiite melts at large depths. At the second stage, already uplifted volcanic buildup ejected mugearite–trachybasaltic lavas, which are characterized by strong vesicularity, heterogeneous distribution and intricate shape of vesicles, and fluidal structure of the rocks.

Basalts dredged from the slopes of the Atlantis and Cruiser seamounts resemble those of basalts of these two volcanic stages in terms of structure and composition. However, there are no direct grounds (e.g., microfossil assemblage entrapped by lava flows) to exclude their subsynchronous development. Differences in the character of volcanism could be caused by local variations in tectonic settings within a volcanic rise. Basaltic samples dredged from the slopes of the Plato, Small Hyeres, Great Meteor, Small Meteor, and Closs seamounts have both vesicular and porphyritic structure with variable composition of phenocrysts, while the modal proportions and structural relations significantly vary between seamounts (Ribeiro, 2017).

Assumptions derived from the available data require further verification. In particular, basalts from the Small Hyeres seamount slopes have trachytic structure and contain minor amount of olivine and pyroxene (Ribeiro, 2017), which is also typical of Cruiser basalts. Both sea mounts are extreme buildups of the southwestern–northeastern lineament on the southern flank of the volcanic rise (Fig. 1). Without excluding the possible higher maturity of these basalts, we may suggest that the style of eruptions depended on the spatial position of extensional area.

The presence of altered humic material on the Cruiser seamount indicates in support of the later volcanic activity. Its accumulation in the shallow lagoonal–marine conditions could not precede the formation of volcanic buildup. Moreover, the accumulation and maturation of humus required sufficient time and appropriate sedimentation setting.

Results of our studies allowed us to link the studied sediments with the second phase of volcanic activity. This follows from the structural-textural features of lava flows (glassy and vesicular groundmass and viscous-ductile deformations) and significant secondary alterations, including the development of clay minerals, zeolites, carbonates, and phosphates in vesicles and other cavities up to their pervasive replacement by palygorskite.

Tectonovolcanic Rises as an Attribute of the Atlantic–Arctic Rift System

Uncertainty with genesis of the tectonosedimentation system of the Atlantis–Meteor seamounts is partially related to the fact that the existing models of its evolution are confined directly to the studied object and are of local application. Even consideration of the hot spot or analysis of influence of the Azores plume on the system evolution does not go beyond the scope of regional studies.

An alternative approach consists in the consideration of structural ensemble of the given region as a part of numerous volcanic buildups, the development of which is tightly related to the progressive crustal extension in the Atlantic–Arctic Rift System (AARS). This system is a divergent boundary about 1800 km long extending from the Bouvet triple point up to the Iceland plume, the main plume of the Arctic zone, and further northward through the Knipovich and Gakkel ridges. The AARS has a frontal junction with Eurasia near the Lena River mouth. Judging from seismicity (Avetisov, 1996), the continuation of the divergent boundary into the continent has a diffuse character and its exact geometry has not been determined yet.

The AARS comprises crustal segments with spreading age varying from 170 Ma in the central segment to 54 Ma in the Arctic segment (Sokolov, 2017). These differences reflect a general evolution of the AARS from the south northward through the pole, but clear decreasing age sequence is not observed.

An important feature of the AARS is the presence of magmatic and amagmatic segments (Lundin et al., 2018). This phenomenon is best expressed in the youngest Arctic segment, where pre-spreading igneous provinces were established along the periphery of surrounding continents. They are traced from the Siberian traps through the high Arctic to modern Iceland (Gaina et al., 2014). Understanding the general tendency is complicated by the fact that igneous provinces in the same oceanic segments have also been formed after spreading initiation. They include the Azores Archipelago and AARS seamounts in its framing. This indicates a pulsed influx of the deep-seated material. Mechanism of the spreading systems–plumes interaction is likely universal and can be exemplified by seamounts surrounding the Azores.

The planetary scale of these processes follows from the potential number, position, and morphological characteristics of seamounts (Morato et al., 2013). Only within the Oslo–Paris Convention for the Protection of the Marine Environment of the North-East Atlantic (OSPAR)-protected territory, 557 large seamounts standing more than 1000 m above sealevel were mapped in the northeastern Atlantic. This list is not complete, because it is constrained by the tasks of studies and parameters applied to reveal the submarine structures. The number of objects will be at least doubled by adding seamounts located along AARS to the south and north of the OSPAR-protected territory.

Based on the spatial position, the seamounts can be subdivided into two principle groups. The first, largest group includes seamounts localized in rift valleys or along their walls, including the along-axial Arctic volcanic structures from the Reykjanes to the Gakkel rifts. It is noteworthy that the intensity of their evolution and distribution density on seafloor practically does not depend on the spreading rate. The well-arranged volcanic buildups and active volcanoes were found in the ultraslow spreading ridges such as the Knipovich and Gakkel rifts.

The second group includes seamounts located at significant distance from rift valleys and shows no obvious link to the main tectonic lineaments—the passive parts of transform faults. However, in some cases, these seamounts are grouped into chains oriented at different angles relative to spreading. Seamounts framing the AARS axis were formed through the interaction of prograding rift system with the pulsed supply of deep-seated melts. The latter could be discharged either in the rift axis or in its framing, thus forming volcanic buildups of the younger age relative to their protolith. The spatial distribution of the superimposed volcanism can be controlled by different factors such as the fault system of transform or regmatic nature. This scenario of intraplate magmatism operates in the basins of all AARS magmatic segments.

One of the main tendencies in the AARS evolution is the formation of paired objects located symmetrically relative to the rift valley. For instance, the Sierra-Leone–Ceara paired rise system in the Equatorial Atlantic forms a symmetrical (bulls eyes) pattern of minima of the anomalous magnetic field (AMF). Such configuration could be formed owing to the short-term intersection of a plume branch with the MAR axis and the short-term pulsed melt influx along this branch with the subsequent quiescence of magmatic activity. A displacement of continuing activity of the AARS plume axis results in the Rio Grande–Walvis ridge type configuration. The present-day active plumes near the AARS axis could be supplied through several pathways in the upper mantle and form seamount chains in the framing. Analysis of AMF between the Atlantis and Vema faults located, respectively, in the Northern and Southern (Equatorial) Atlantic allowed us to reveal six paired zones relative to MAR (Sokolov, 2017). Analysis of small (<50 km) equant negative gravity anomalies within the MAR flanks showed that they correspond to paired landforms that are symmetric relative to the rift valley. A bright example of such anomalies is a chain consisting of three pairs and one central anomaly immediately south of the Strakhov Fault (4° N). Paired structures of different scale were also established in the Arctic segment of the AARS, in the young oceanic structures restricted to the Norwegian Greenland and Arctic provinces, which mark the North Atlantic continuation. For instance, the local paired landforms are the Litvin and Pogrebitsky seamounts located, respectively, on the western and eastern flanks of the Knipovich rift valley (Chamov et al., 2010).

The geographic position, structure, and composition of basalts of the Atlantis–Meteor tectonosedimentation system are well consistent with the above mentioned models of the formation of within-plate volcanism on different AARS segments both in the plume axis and off-axis, with allowance for the displacement of plate systems relative to the deep pathways of mantle material. The Atlantis–Meteor system is the eastern part of the paired structure ensemble that is symmetrical relative to the AARS rift valley, the western flank of which composes the Corner seamount group. Both parts of the former ensemble are located on flanks of the Oceanographer, Hayes, and Alantis transform faults, which are spaced from each other at about 2000 km and are marked by 34 paired magnetic anomalies (Roest et al., 1992).

Due to the best structural conjugation of the Corner, Plato, and Cruiser seamount groups along the Hayes Fault, the latter can be considered as axis of the entire transform fault system. Available data allowed us to relate the initiation of the system and the development of these linear extension zones and subsequent volcanism with the decompression melting of the underlying mantle beneath them. The rift axis is not displaced along these faults, which is not typical of AARS and can be related to the affiliation of the system to the central segment with the longest evolution and maximum opening.

CONCLUSIONS

The study of rocks dredged from the Atlantis, Plato, and Cruiser seamounts allowed us to reconstruct volcanic and sedimentation settings that have existed in this area in the Miocene.

Basalts of the Atlantis and Cruiser seamounts were formed in different settings. Well-crystallized vesicle-free olivine basalts of the Atlantis Seamount resulted from the deep-water eruptions under high pressure. Their eruption at great depths is also supported by the taxonomic composition (typical of open basins) of microfauna entrapped with the bottom sediments. Well-pronounced chill margins indicate a sharp temperature contrast on their contact with sediments. The Cruiser basalts show amygdaloidal structure typical of the shallow subaerial eruptions, which produce relatively thin and highly vesicular hyalobasaltic flows. In addition, the basalts contain inclusions of the terrigenous–humic material of subaerial origin. Differences in the conditions of basaltic eruptions could be caused by both local variations in tectonic settings within the volcanic rise and by the temporal evolution of melts from ankaramite to mugearite.

The absence of marine microfauna in the cement of tuffogenic sediments from the Plato Seamount likely indicate that they were formed under subaerial conditions. Tuff breccias were formed by the compaction and cementation of the unsorted coarse-clastic loose volcaniclastic material in the sand-sized tuff cement. Facies similarity of tuff gravelstones with alluvial–proluvial sediments of temporal water streams also supports the subaerial sedimentation settings.

The study of terrigenous–humic sediments of the Cruiser Seamount indicates subaerial sedimentation settings in the past. The laminated texture of the organogenic–terrigenous mass points to its multistage accumulation in a semi-isolated shallow marine basin with periodical influx of the terrigenous material and plant fragments. The sediments are mainly composed of fragments of the terrestrial higher plants (remains of shrubs, tree branches), which follows from a clear cellular structure of plant tissues. The shallow marine plant material (calcareous algae and algal mats) occurs in subordinate amount. The fact that the basin was partly isolated from ocean is confirmed by the poor taxonomic composition of microfauna. The absence of traces of active water dynamics and the pelite size of terrigenous material point to the quiescent sedimentation setting. Such conditions could arise in a shallow-water bay (lagoon), which served as the local depocenter for the adjacent volcanic buildups.

The study of material dredged from the eastern slope of the Cruiser Seamount indicates that the shal-

low-water terrgenous–humic lagoonal marine sediments were subjected to the high-temperature impact of subaerial lava flows. Widespread stellate segregations of fusinite and pyrofusinite indicate that the organic matter acquired anisotropic properties under the high-temperature impact. Analysis of the chemical composition of rocks showed that the lignite matter made up mainly of the higher plant fragments under high temperature lost volatiles and mobile elements and was transformed into the highly carbonaceous natural coke. The mobile, CO_2-saturated fluids penetrated the laminas with the terrigenous and likely sapropel material and facilitated the leaching and redeposition of some components. The removal of Fe, Ca, Na, Si and, to lesser extent, K led to the enrichment of sediments in CO_2.

Based on available data, the studied sediments are related to the final Late Miocene–Pliocene volcanic stage in the seamount system. This stage preceded the destruction of system, its prograde subsidence, and transformation of islands into guyots.

ACKNOWLEDGMENTS

We are grateful to the team of the R/V *Akademik Nikolai Strakhov* for help in the performance of studies.

We thank G.N. Aleksandrova (Geological Institute, Russian Academy of Sciences), N.V. Pronina, and A.E. Terent'eva (Moscow State University) for valuable comments.

FUNDING

This work was supported by the State Task of the Geological Institute of the Russian Academy of Sciences, project nos. 0135-2018-0034 and 0135-2019-0069 (Tectonosedimentation Analysis), 0135-2019-0070 (Study of Organic Matter), and AAAA-A17-117030610119-6 (Paleontological Analysis). The position of tectonovolcanic rises within the Atlantic–Arctic Rift System was analyzed with support of the Russian Foundation for Basic Research, project no. 18-05-70040 (Arctic Resources).

REFERENCES

Avetisov, G.P., *Seismoaktivnye zony Arktiki* (Seismoactive Zones in the Arctic), St. Petersburg: VNIOG, 1996.

Bebeshev, I.I., Zolotarev, B.P., Eroshchev-Shak, V.A., et al., *Vulkanicheskie podnyatiya i glubokovodnye osadki vostoka Tsentral'noi Atlantiki* (Volcanic Rises and Deep-Water Sediments in the Central Atlantic), Moscow: Nauka, 1989.

Chamov, N.P., Sokolov, S.Yu., Kostyleva, V.V., et al., Structure and composition of the sedimentary cover in the Knipovich Rift Valley and Molloy Deep (Norwegian–Greenland Basin), *Lithol. Miner. Resour.*, 2010, no. 6, pp. 532–554.

Duin, E.J.Th., Some geophysical characteristics of the lower southwest flank of the Cruiser-Hyers seamount group, eastern North Atlantic, *Mededel. Rijks Geol. Dienst*, 1984, vol. 38, no. 2, pp. 39–49.

Gaina, C., Medvedev, S., Torsvik, T.H., et al., 4d Arctic: A glimpse into the structure and evolution of the Arctic in the light of new geophysical maps, plate tectonics and tomographic models, *Surv. Geophys.*, 2014, vol. 35, pp. 1095–1122.
https://doi.org/10.1007/s10712-013-9254-y

Gente, P., Dyment, J., Maia, M., and Goslin, J., Interaction between the Mid-Atlantic Ridge and the Azores hot spot during the last 85 Myr: Emplacement and rifting of the hot spot-derived plateaus, *Geochem. Geophys. Geosyst.*, 2003, vol. 4, no. 10, pp. 1–23.

Georgen, J.E., Lithospheric control on the spatial pattern of Azores hotspot seafloor anomalies: Constraints from a model of plume-triple junction interaction, *Geophys. Rev. Lett.*, 2011, vol. 38, L19305, pp. 1–6.

Golovina, L.A., Shipunov, S.V., Muzylev, N.G., and Shmidt, O.A., Stratigraphy based on nannoplankton and paleomagnetism of bottom sediments in the Eastern Atlantic, in *Vulkanicheskie podnyatiya i glubokovodnye osadki vostoka Tsentral'noi Atlantiki* (Volcanic Rises and Deep-Water Sediments in the Eastern Central Atlantic), Moscow: Nauka, 1989, pp. 76–89.

Heaman, L.M. and Kjarsgaard, B.A., Timing of eastern North American kimberlite magmatism: continental extension of the Great Meteor hotspot track?, *Earth Planet. Sci. Lett.*, 2000, vol. 178, pp. 253–268.

Irvine, T.N. and Baragar, W.R.A., A guide to the chemical classification of the common volcanic rocks, *Can. J. Earth Sci.*, 1971, vol. 8, pp. 523–548.

LeBas, M.J., LeMaitre, R.W., Streckeisen, A., and Zanettin, B., A chemical classification of volcanic rocks based on the total alkali-silica diagram, *J. Petrol.*, 1986, vol. 27, pp. 745–750.

Lundin, E.R., Dore, A.G., and Redfield, T.F., Magmatism and extension rates at rifted margins, *Petrol. Geosci.*, 2018, vol. 24, pp. 379–392.

Mironov, A.N. and Krylova, E.M., Origin of the fauna of the Meteor Seamounts, north-eastern Atlantic, in *Biogeography of the North Atlantic Seamounts*, Mironov, A.N., Gebruck, A.V., and Southward, A.J., Eds., Moscow: KMK Sci. Press, 2006, pp. 22–57.

Morato, T., Kvile, K.Ø., Taranto, G.H., et al., Seamount physiography and biology in the north-east Atlantic and Mediterranean Sea, *Biogeosciences*, 2013, vol. 10, pp. 3039–3054.

Peive, A.A. and Chamov, N.P., Basic tectonic features of the Knipovich Ridge (North Atlantic) and its neotectonic evolution, *Geotectonics*, 2008, no. 1, pp. 31–47.

Petrova, V.V., Stukalova, I.E., and Sulerzhitskii, L.D., Humic organic matter transformation during the interaction with pyroclastic material, *Lithol. Miner. Resour.*, 1998, no. 4, pp. 380–386.

Ribeiro, L.P., Martins, S., Hildenbrand, A., et al., The genetic link between the Azores Archipelago and the Southern Azores Seamount Chain (SASC): The elemental, isotopic and chronological evidences, *Lithos*, 2017, vol. 294/295. pp. 133–146.

Roest, W.R., Daiñobeitia, J.J., Verhoef, J., and Collette, B.J., Magnetic anomalies in the Canary Basin and the Mesozoic

evolution of the Central North Atlantic, *Mar. Geoph. Res.*, 1992, vol. 14, pp. 1–24.

Stach, E., Mackowsky, M.-Th., Teichmüller, M., Taylor G.H., et al., *Coal Petrology*, Berlin, 1975. Translated under the title Petrologiya uglei, Moscow: Mir, 1978.

Sokolov, S.Yu., *Tektonika i geodinamika Ekvatorial'nogo segmenta Atlantiki* (Tectonics and Geodynamics of the Equatorial Atlantic segment), Moscow: Nauchn. Mir, 2017.

Stukalova, I.E., Rusinova, O.V., and Syngaevskii, E.D., Thermal alteration of coals in the Khasyn deposit (Magadan region), in *Geologiya ugol'nykh mestorozhdenii* (Geology of Coal Fields), Yekaterinburg: UGGU, 2004, iss. 14, pp. 199–208.

Tucholke, B.E. and Smoot, N.C., Evidence for age and evolution of Comer seamounts and Great Meteor seamount chain from multibeam bathymetry, *J. Geophys. Res.*, 1990, vol. 95, no. B11, pp. 17555–17569.

Verhoef, J., A geophysical study of the Atlantis-Meteor seamount complex, *Geol. Ultraiectina*, 1984, vol. 38, pp. 1–151.

Wendt, I., Kreuzer, H., Muller, P., et al., K-Ar age of basalts from Great Meteor and Josephine seamounts (eastern North Atlantic), *Deep-Sea Res.*, 1976, vol. 23, pp. 849–862.

Willians, C.A., Verhoef, J., and Collette, B.J., Magnetic analysis of some large seamounts in the North Atlantic, *Earth Planet. Sci. Lett.*, 1983, vol. 63, no. 3, p. 399.

Zolotarev, B.P., Eroshchev-Shak, V.A., Gutsaki, V.A., and Rikhter, A.A., Volcanism in the Cruiser and Krylov seamounts and hydrothermal alterations of rocks in them, in *Vulkanicheskie podnyatiya i glubokovodnye osadki vostoka Tsentral'noi Atlantiki* (Volcanic Rises and Deep-Water Sediments in the Central Atlantic), Moscow: Nauka, 1989, pp. 95–111.

Translated by M. Bogina